Research

Dielectric and energy harvesting properties of functionalized composite nanofibers consisting of Boc-Phe-Leu self-assembled dipeptide inclusions in biocompatible polymeric matrices

Adelino Handa[1] · Rosa M. F. Baptista[1] · Daniela Santos[1] · Bruna Silva[1] · João Oliveira[1] · Bernardo Almeida[1] · Etelvina de Matos Gomes[1] · Michael Belsley[1]

Abstract

Hybrid bionanomaterials were produced through electrospinning, incorporating the dipeptide Boc-ʟ-phenylalanyl-ʟ-leucine into nanofibers of biocompatible polymers. Scanning electron microscopy confirmed the uniformity of the nanofibers, with diameters ranging from 0.56 to 1.61 μm. The dielectric properties of the nanofibers were characterized using impedance spectroscopy, assessing temperature and frequency dependencies. Notably, the composite micro/nanofibers exhibited semiconducting dielectric behavior with bandgap energies of 4–5 eV, and their analysis revealed increased dielectric constant with temperature due to enhanced charge mobility. The successful incorporation of the dipeptide was verified by Maxwell–Wagner interfacial polarization, and the Havriliak–Negami model disclosed insights into electric permittivity. Furthermore, the fibers demonstrated pyroelectric and piezoelectric responses, with Boc-Phe-Leu@PLLA nanofibers having the highest piezoelectric coefficient of 85 pC/N. These findings highlight the influence of dipeptide nanostructures on dielectric, pyroelectric, and piezoelectric properties, suggesting the potential of polymeric micro/nanofibers as efficient piezoelectric energy generators for portable and wearable devices.

✉ Michael Belsley, belsley@fisica.uminho.pt | [1]Centre of Physics of Minho and Porto Universities (CF-UM-UP), Laboratory for Materials and Emergent Technologies (LAPMET), University of Minho, Campus de Gualtar, 4710-057 Braga, Portugal.

Graphical Abstract
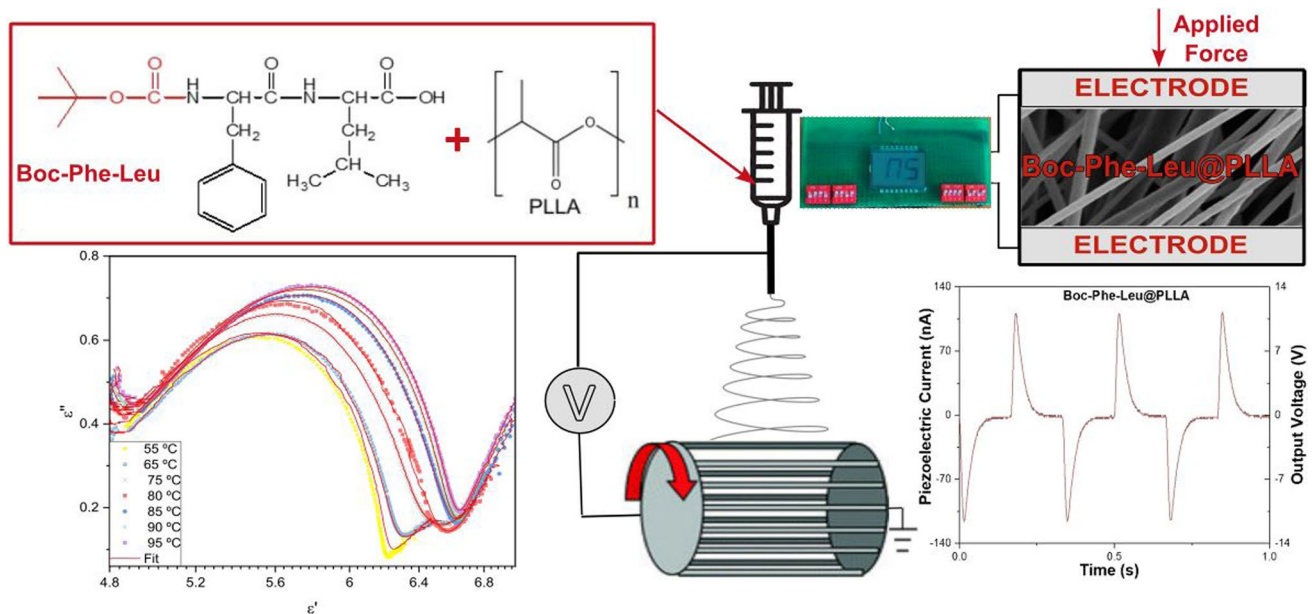
1 Introduction

The rapid advancement of science and technology has led to significant growth in the development of new materials with diverse applications across industries and high technology. As portable microelectronic devices become increasingly prevalent, the search for efficient power sources has intensified. Since rechargeable batteries, commonly used in current detection systems, may not be optimal for miniature devices used in various sectors, like health monitoring, safety, transportation, and surveillance, extensive research has been focusing on exploring alternative solutions [1, 2].

To fully harness the potential of nanomaterials, it is essential to understand their properties and investigate their applications. Peptide nanomaterials offer a range of desirable characteristics, including thermal and mechanical stability, electrical conductivity, piezoelectricity, and optical properties, making them suitable for incorporation into (nano) devices. When dipeptide nanomaterials are integrated into polymeric nanofibers, they create new composite-based materials that exhibit enhanced thermal and mechanical stability [3, 4]. These dipeptides can be easily modified through functionalization, resulting in bioinspired and durable semiconductor/dielectric materials.

Peptide nanomaterials, known for their ability to self-assemble, hold tremendous potential in various fields, particularly in medical applications, such as controlled drug administration, and in microelectronics, which could significantly impact our future daily lives. Due to their biomimetic characteristics [3, 5], peptides can form a wide range of structures that can be utilized for manufacturing functional devices [6].

By purposefully designing different amino acid sequences, peptides, which are natural compounds composed of specific molecular structures, can exhibit diverse self-assembling properties. These properties allow dipeptide nanomaterials to form a variety of nanostructures at the nanoscale, including nanotubes, nanospheres, nanofibrils, nanoribbons, and other ordered structures [6–10]. Their flexibility and variability in molecular design make them essential molecular building blocks with broad applications [11].

Studying the dielectric properties of amino acids and dipeptides is vital for understanding their electrical behavior, optimizing their performance in electronic and energy storage devices, and uncovering their molecular dynamics and intermolecular interactions.

Fig. 1 Chemical structure of chiral dipeptide Boc-Phe-Leu
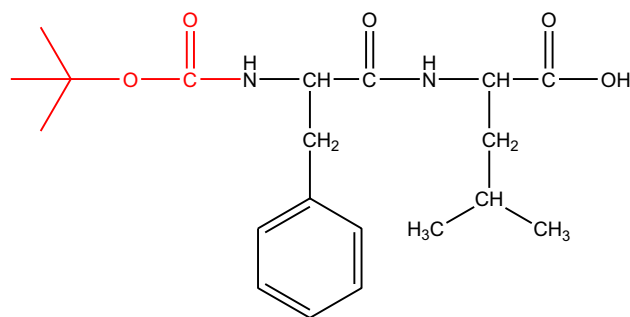
In our specific research, we focus on investigating the electrical behavior of *tert*-butoxycarbonyl-L-phenylalanyl-L-leucine (Boc-L-phenylalanine-L-leucine-OH, hereafter Boc-Phe-Leu) dipeptide nanostructures within a fibrous matrix—(see Fig. 1). Previous studies have shown modifications in vibronic modes and enhanced molecular polarizability in amino acid L-leucine due to hydrogen bonds [12, 13]. Other factors beyond zwitterionization may contribute to this enhancement. Molecular geometry plays a significant role, as evidenced by similar polarizability levels in L-leucine and L-isoleucine.

Piezoelectricity and pyroelectricity are essential properties of non-centrosymmetric biomaterials, with broad applications. Piezoelectricity enables the conversion of mechanical energy into electrical energy [14], while pyroelectricity responds to temperature changes [4]. Understanding and optimizing these properties in biomaterials, such as amino acids and dipeptides, has been crucial for advancing biomaterial development [5, 15–18]. More recently, the piezoelectric properties of L-leucine crystalline films were comprehensively characterized through a combination of extensive measurements, density functional theory calculations, and optical microscopy [19].

In our prior research, we detailed the integration of three Boc-protected analogues of the PhePhe (L-phenylalanyl-L-phenylalanine) dipeptide into micro- and nanostructured fibers of PLLA (Poly-L-lactic acid) polymer. These analogues comprise Boc-PhePhe, Boc-*p*-nitro-L-phenylalanyl-*p*-nitro-L-phenylalanine (Boc-pNPhepNPhe), and Boc-L-phenylalanyl-L-tyrosine (Boc-PheTyr). Our investigation involved their self-assembly within the polymer matrix and showcased the generation of elevated piezoelectric voltages through the piezoelectric effect. It is worth noting that this incorporation of dipeptides yielded an augmentation in the piezoelectric response of the PLLA polymer, which inherently possesses piezoelectric properties [6, 11]. The selection of Boc-Phe-Leu arises from its derivation from the extensively studied Phe-Phe dipeptide, which is recognized for its piezoelectric properties. By studying a dipeptide within the same family but with the substitution of an aromatic (Phe) for an aliphatic (Leu) side-chain amino acid, we aimed to explore the resulting variations in piezoelectric behaviour. This inquiry allowed us to investigate how distinct molecular structures within the dipeptide family can influence the resulting piezoelectric, pyroelectric, and dielectric properties in our hybrid bionanomaterials. This work not only links our understanding of dielectric properties and the exploration of piezoelectric behaviour in dipeptide nanofibers but also sets the stage for further advancements in biomaterial development and energy harvesting. This advancement holds promise for the creation of sustainable, innovative, and biocompatible technologies and applications.

2 Materials and methods

2.1 Materials

L-Phenylalanyl-L-leucine (Phe-Leu) and di-*tert*-butylpyrocarbonate (Boc$_2$O) were purchased from Bachem (Muenchenstein, Switzerland) and Alfa Aesar (Erlenbachweg, Germany) and used as received.

In this project, three different polymers were selected to create the fibers: poly-L-lactic acid (PLLA, Mw 217–225,000), which was obtained from Corbion (Gorinchem, Netherlands), Polycaprolactone (PCL, Mw 80,000) and Poly (methyl methacrylate) (PMMA, Mw 996,000), both of which were purchased from Merck/Sigma-Aldrich (Darmstadt, Germany).

To dissolve the polymers and dipeptide, several solvents were used, including dichloromethane (DCM), *N, N*-dimethylformamide (DMF), and chloroform, all of which were acquired from Merck/Sigma-Aldrich, and 1,4-dioxane, which was obtained from Fisher Chemicals (Zurich, Switzerland).

Boc-Phe-Leu dipeptide was functionalized using standard protecting group chemistry to introduce a conventional Boc (*tert*-butyloxycarbonyl) protecting group [20]. The Boc group was employed for N-terminal protection of the Phenylalanine amino acid within the Phe-Leu dipeptide.

To initiate the functionalization process, 2 g of Phe-Leu were dissolved in a mixture of 1,4-dioxane (20 mL), water (12 mL), and 1 M sodium hydroxide (NaOH) solution (12 mL). The resulting solution was stirred at a rate of 500 rpm and cooled to 0 °C using an ice-water bath for a duration of 20 min. Following complete homogenization of the solution, di-*tert*-butylpyrocarbonate (1.72 g, 1.1 eq.) was introduced, and stirring was sustained at room temperature for 40 h. Subsequent to this reaction period, the reaction mixture was overlaid with a layer of ethyl acetate (50 mL) and acidified with a diluted solution of potassium hydrogen sulfate, $KHSO_4$ (6.31 g, 50 mL), to achieve a pH of 2–3 (validated using Congo red indicator). Stirring of the solution was maintained, and the aqueous phase was separated following repeated washes with ethyl acetate. The ethyl acetate was evaporated from the organic phase, resulting in the formation of Boc-Phe-Leu in the form of a white solid. This solid was subsequently subjected to drying in an oven at 50 °C during 24 h.

To ascertain the chemical structure of the boc-protected dipeptide, Boc-Phe-Leu, nuclear magnetic resonance (NMR) spectroscopy was performed on a Bruker Avance III 400 instrument operating at a frequency of 400 MHz for [1]H.

2.2 Polymerics solutions and electrospinning of micro/nanofibers

To prepare the polymeric solution, 10% PLLA (w/v) was dissolved in DCM at a temperature of 35 °C and stirred at a speed of 600 rpm until it was completely dissolved. The dipeptide was then dissolved in DMF and added to the previous solution at a solvent ratio of 4:1 (v/v) while stirring at a speed of 300 rpm at room temperature for 24 h. A similar method was used to prepare 10% PMMA without any addition of temperature. On the other hand, the polymeric solution of 10% PCL (w/v) in DCM was subjected to an agitation of 600 rpm, at room temperature, throughout the dissolution process, and the DMF was added later in the proportion 4:1 (v/v). In this sample, the dipeptide was dissolved in DCM/chloroform in the proportion 1:1 (v/v) and added drop by drop to the polymer solution after the total dissolution of the polymer.

For electrospinning, a precursor solution was loaded into a syringe with a 0.232 mm inner diameter needle (0.5 mm outer diameter), where the high-voltage power supply is applied (Spellmann CZE2000, Bochum, Germany). As seen in Fig. 2, the electrospinning device has vertical geometry, and the processes were executed at room temperature and pressure. The collector is cylindrical in shape and rotary and is covered with high purity aluminum foil that will serve as an electrode. Important parameters to have into consideration, to obtain fibers free of beads, include the distance between the needle and the collector (11 cm), the electric potential difference (18–20 kV), and the flow rate of the solution (0.30 mL/h).

2.3 Scanning electron microscopy (SEM)

The morphological characterization of electrospun fibers with embedded Boc-Phe-Leu self-assembled dipeptide was investigated using Scanning Electron Microscopy (SEM). To study the size and shape of the Boc-Phe-Leu fibers (placed

Fig. 2 Representative electrospinning scheme
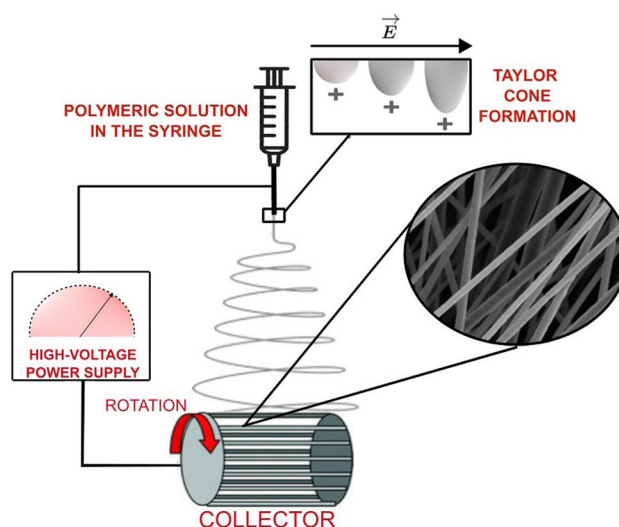
in a silica slide), a Nova Nano SEM 200 was used, at an accelerating voltage of 10 kV. The fiber mats were covered with a film (10 nm) of Au–PD (80–20 w%), using a high-resolution sputter coater (model 208HR from Cressington Company), coupled to Cressington MTM-20 high-resolution thickness controller. The average diameters of the fibers were estimated from SEM images, using ImageJ software [21].

2.4 Diffuse reflectance spectroscopy (UV–VIS)

To study the reflectance of the fiber mats, a UV-2501PC spectrophotometer with an integration sphere (ISR-205 240A), from Shimadzu Corporation, Kyoto, Japan was used in the measurements of the diffuse reflectance spectra. Barium sulphate was used as a reference. A wavelength range of 200–800 nm.

To determine the band gap energy (E_g) of the fiber mats, the Kubelka–Munk function, F(R), was used. The Kubelka–Munk function obeys the relation given by $[h\nu F(R)]^n = \alpha(h\nu - E_g)$, where $h\nu$ is the energy of the incident photon, α is the absorption coefficient and n represents the type of electronic transition. For this work, $n = 1/2$ was used as this is an indirect band gap. F(R) is determined from the total reflectance coefficient of the material (R) by:

$$F(R_\infty) = \frac{(1 - R_\infty)^2}{2R_\infty} = \frac{K}{S} \tag{1}$$

2.5 Dielectric spectroscopy

The dielectric properties of electrospun fibers with embedded Boc-Phe-Leu self-assembled dipeptide inclusions were studied by impedance spectroscopy to gain insights into their electrical behavior, energy storage capabilities, and suitability for various applications. The impedance spectroscopy was measured in the temperature range of 283–383 K and in the frequency range of 20 Hz–3 MHz. The complex permittivity, written as $\varepsilon = \varepsilon' - i\varepsilon''$, where ε and ε'' are the real and imaginary parts, respectively. The values of ε' and ε'' were calculated from the measured capacitance (C) and loss tangent (tan δ), using the equations:

$$C = \varepsilon' \varepsilon_0 (A/d) \text{ and } \tan \delta = \varepsilon''/\varepsilon'.$$

Here A is the electric contact area and d is the fiber mat thickness. To perform the measurements, the samples formed a parallel plate capacitor and were included in an LCR network. To form the capacitor, the aluminum foil, used as the substrate to collect the fiber mats, was the bottom electrode while the top electrode was the base of a cylindrical metal contact, with approximately 10^{-2} m diameter. A Wayne Kerr 6440A precision component analyzer was used together with a dedicated computer and software to acquire the data. Shielded test leads were employed to avoid parasitic impedances due to connecting cables. Temperature-dependent measurements were performed at a rate of 2 °C/min, using a Polymer Labs PL706 PID controller and furnace.

2.6 Pyroelectric coefficient

Pyroelectricity is a phenomenon that results from the temperature dependence of material spontaneous polarization (P_s) in a non-centrosymmetric material. The rate of change of the spontaneous polarization with temperature during heating or cooling, $p = dP_s/dT$, is the pyroelectric coefficient. The change in polarization was detected by measuring the pyroelectric current, I, which is proportional to the rate of change of polarization, using a Keithley 617 electrometer (Keithley Instruments GmbH, Landsberg, Germany). The equation used to calculate the pyroelectric current is I = A (dP_s/dT)(dT/dt), where A is the electrode area and dT/dt is the rate of temperature change. The measurements were performed in a capacitor geometry under short-circuit conditions. The fiber mat sample, with aan rea $\pi \times 5^2$ mm^2 and 20–330 μm thickness, formed a parallel plane capacitor.

2.7 Piezoelectric measurements

The nanofiber mats were directly deposited onto high-purity aluminum sheets, which served as electrodes for piezo-electric measurement. The resulting samples were secured onto a stage, and uniform perpendicular forces were applied across the surface area of each sample. The measured fiber mat arrays had an area of (30×40) mm^2 with a thickness ranging from 20 to 160 µm. They were subjected to periodic mechanical forces generated by a vibration generator (Frederiksen SF2185) with an amplitude of 500 mVpp and a frequency of 3 Hz provided by a signal generator (Hewlett Packard 33120A). Prior to the experiment, the applied forces were calibrated using a force-sensing resistor (FSR402, Interlink Electronics Sensor Technology, Graefelfing, Germany).

The piezoelectric output voltage was measured using a 100 MΩ resistor connected to a 6 dB low-pass filter, followed by a low-noise preamplifier (research system SR560). The voltage values were then recorded by a digital storage oscilloscope (Agilent Technologies DS0-X-3012A). From the applied force time interval, Δt, and knowing the maximum piezoelectric current, the value of the charge, Q, was determined through the equation $Q = I_{max}\Delta t$. The effective piezoelectric coefficient, d$_{eff}$, was obtained taking into account the charge Q and the applied force F$_{ap}$, through equation $d_{eff} = Q/F_{app}$. A piezoelectric nanogenerator is manufactured by employing an electrospun fiber mat of Boc-Phe-Leu@PLLA. The process involves the direct deposition of this electrospun fiber mat onto high-purity aluminum sheets during the electrospinning procedure. These sheets serve as both top and bottom electrodes, each
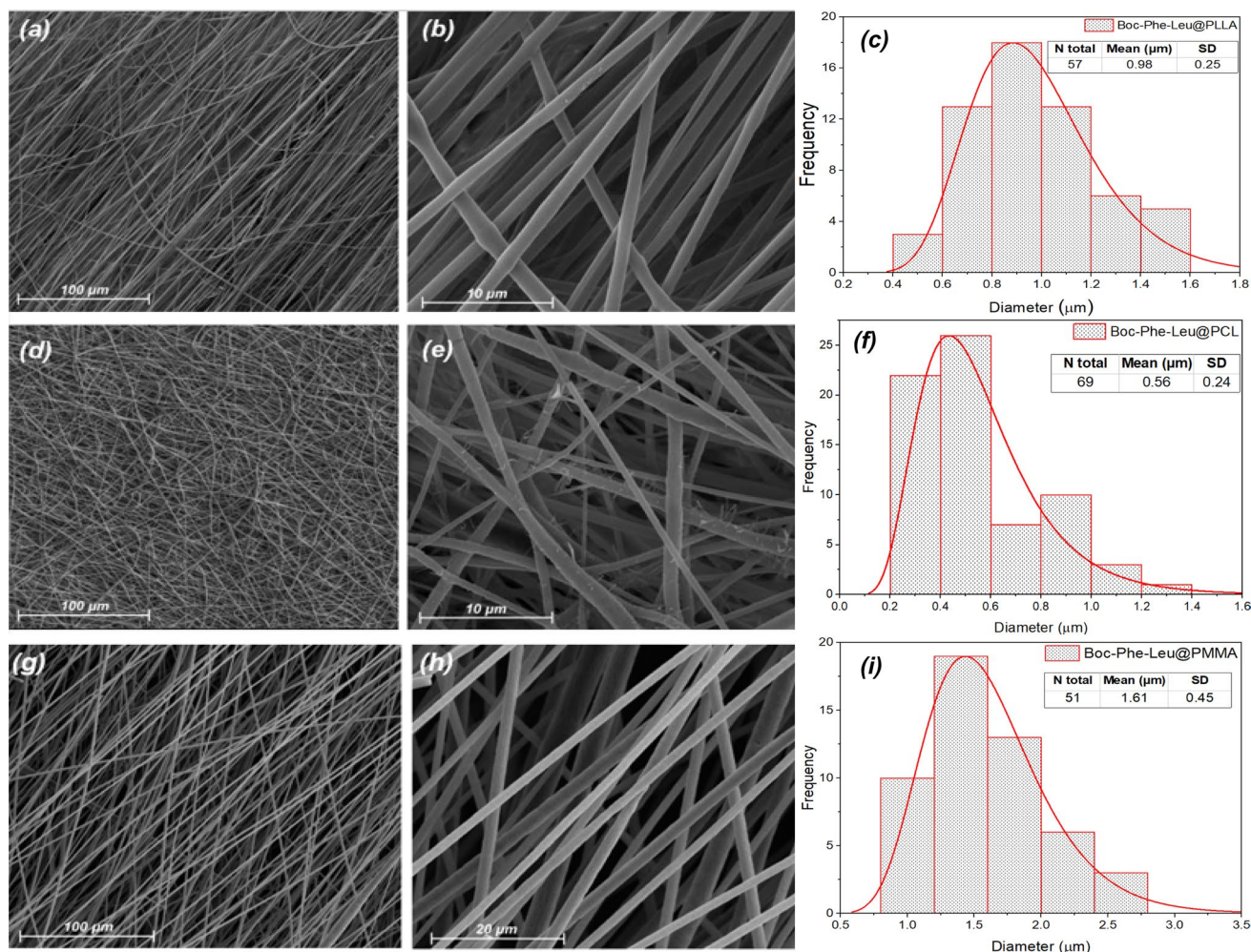

Fig. 3 SEM images at magnification levels of 1000×, 5000×, 10,000×, and 50,000× and the respective fiber diameter distribution histograms for PLLA (**a–c**), PCL (**d–f**), and PMMA (**g–i**) with embedded Boc-Phe-Leu chiral dipeptide. The blue curves indicate lognormal distributions using the mean, maximum, and standard deviations of each set of fibers

covering an area of (30×40) mm^2. Following this, copper wires were attached to these electrodes as well as to the conductors of the LCD screen, as represented in Fig. 13.

3 Results and discussion

3.1 Morphology of electrospun fibers

Figure 3 shows SEM micrographs of the fibers for the different polymers with the incorporated Boc-Phe-Leu dipeptide, with their histograms representing the diameters of the microstructures. The Boc-Phe-Leu@PLLA images (Fig. 3a–c) show clear and uniform fibers with an average diameter of 0.98 µm, while Boc-Phe-Leu@PMMA (Fig. 3g–i) has much larger diameters in the order of 1.68 µm. For Boc-Phe-Leu@PCL (Fig. 3d–f), the SEM images show an average diameter of 0.56 µm, due to PCL's excellent processability and chains flexibility, resulting in a smaller diameter with the confinement of the embedded dipeptide. The alignment of fibers during the electrospinning process depends on variables such as the rotational speed of the collector, the applied voltage, the viscosity of the precursor solution, and other dynamic process parameters. In the scanning electron microscopy (SEM) images (Fig. 3a, b, g, h), a discernible preferred orientation can be observed for the Boc-Phe-Leu@PLLA and Boc-Phe-Leu@PMMA fibers. On the other hand, the Boc-Phe-Leu@PCL fibers (Fig. 3d and e) exhibit a relatively more random orientation in comparison.
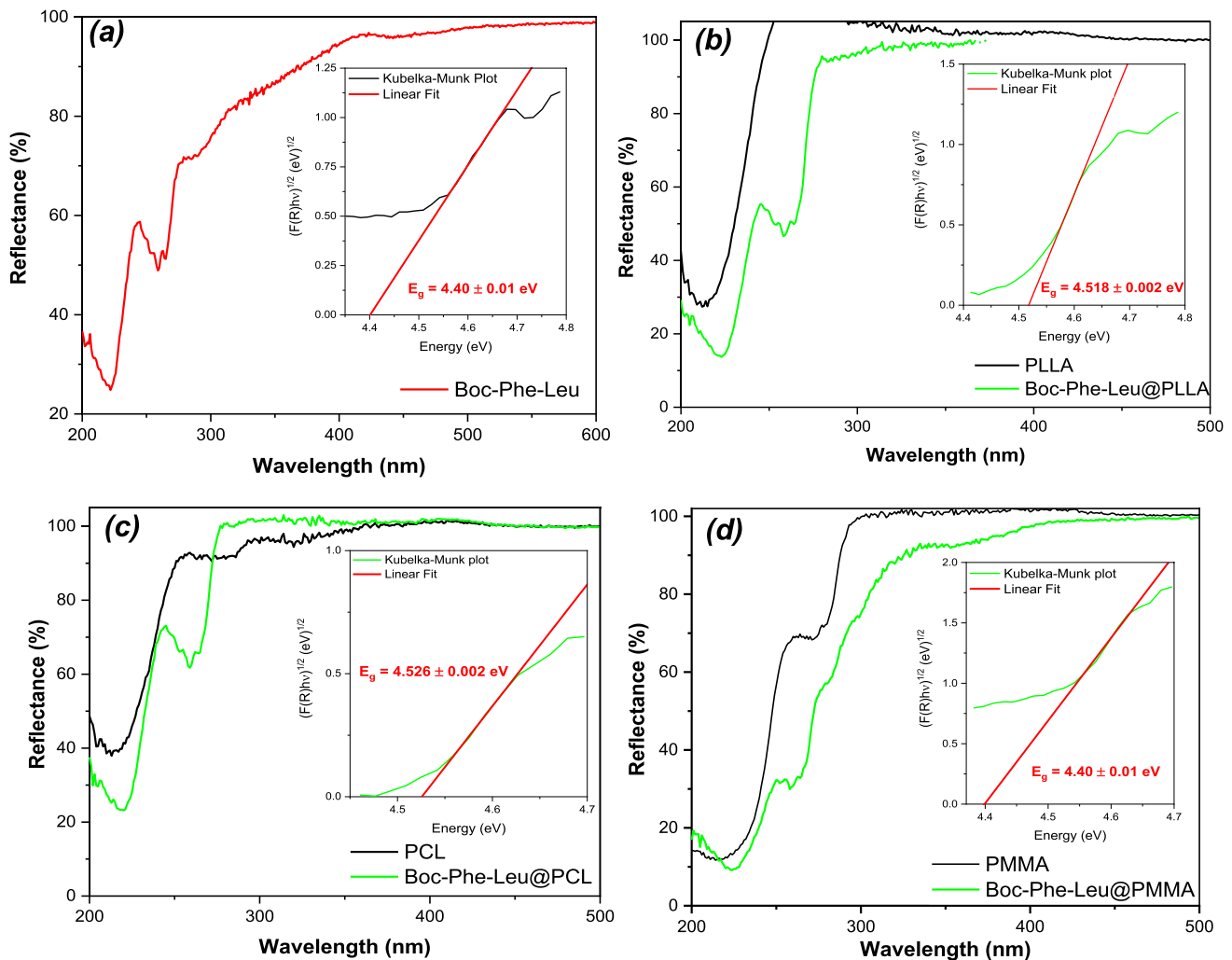

Fig. 4 Reflectance spectra of **a** Boc-Phe-Leu dipeptide, **b** Boc-Phe-Leu@PLLA fibers, **c** Boc-Phe-Leu@PCL fibers, and **d** Boc-Phe-Leu@PMMA fibers. The inset shows the band gap energy determined from the Kubelka–Munk function with the linear fit in red

3.2 Band gap energy

In Fig. 4, the reflectance spectra of the Boc-Phe-Leu dipeptide (Fig. 4a) and Boc-Phe-Leu embedded into polymers fibers (Fig. 4b–d), are reported. The band gap (E_g) was determined from them, through a Kubelka–Munk plot, as shown in the insets of the figures. The result indicates an energy of $E_g = 4.40 \pm 0.01$ eV for Boc-Phe-Leu. When the dipeptide is incorporated into polymeric fibers, there is an increase in band gap energy, attaining values of 4.518 ± 0.002 eV and 4.526 ± 0.002 eV for PLLA and PCL fibers, respectively. This shows a clear influence of the incorporation of the dipeptidic material inside the polymeric fibers. The Boc-Phe-Leu@PMMA band gap energy remains the same as the dipeptide alone.

3.3 Dielectric properties

The frequency dependence of the permittivity of the composite polymeric nanofibers with Boc-Phe-Leu dipeptide inclusions, was measured between room temperature and 373 K for the mats with different polymeric fiber matrices. Figures 5a–c and 6a–c show the real and imaginary components of the dielectric permittivity for the samples with Boc-Phe-Leu@PLLA, Boc-Phe-Leu@PCL and Boc-Phe-Leu@PMMA fibers, respectively. From the analysis of the real electric permittivity data of the nanofibers, it was possible to observe that the application of an electric field induces significant polarization at low frequency, resulting in an increasing ε′ with decreasing frequency. This is due to the
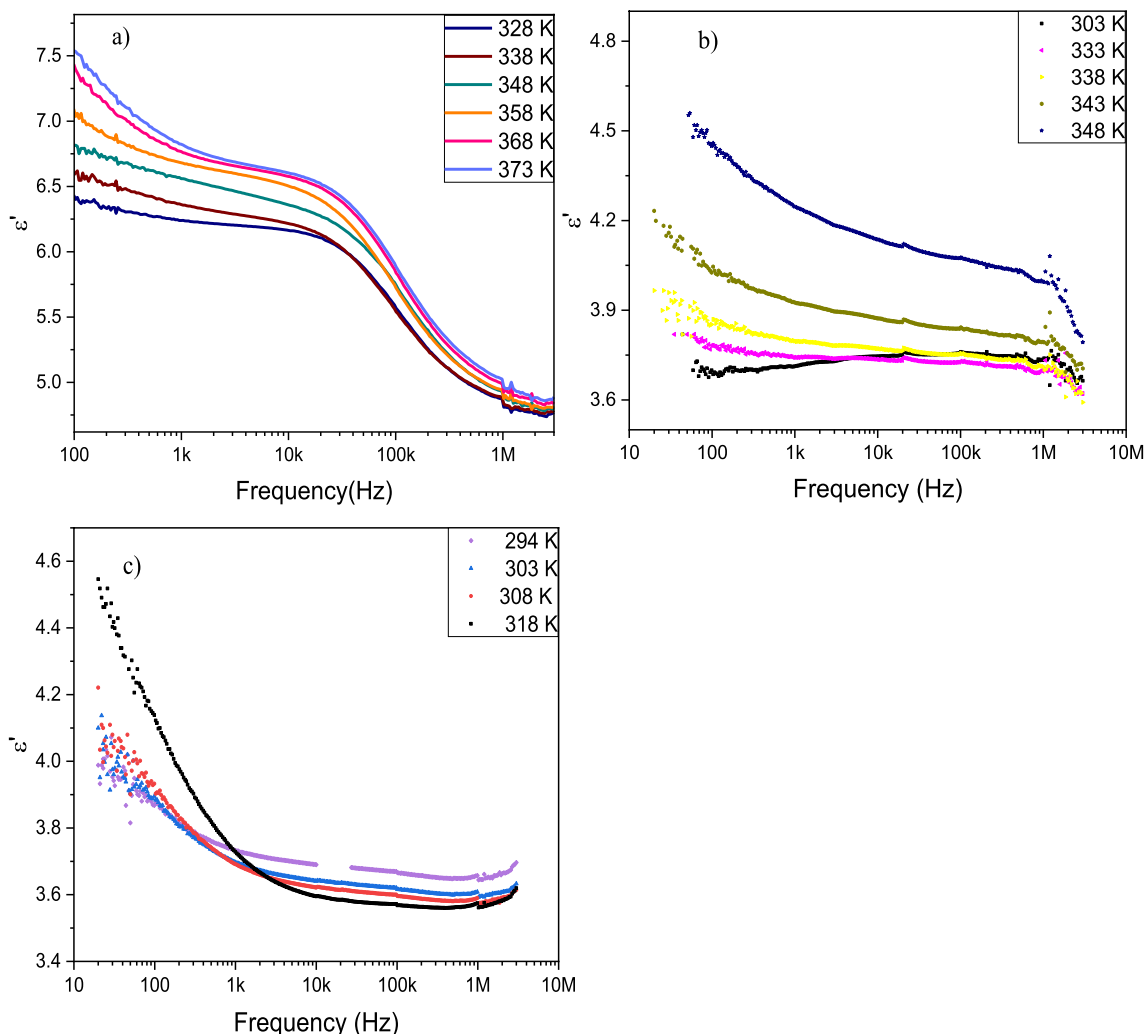
Fig. 5 Frequency dependence of the real part of the dielectric permittivity, measured at different temperatures on the **a** Boc-Phe-Leu@PLLA, **b** Boc-Phe-Leu@PMMA, and **c** Boc-Phe-Leu@PCL fibers
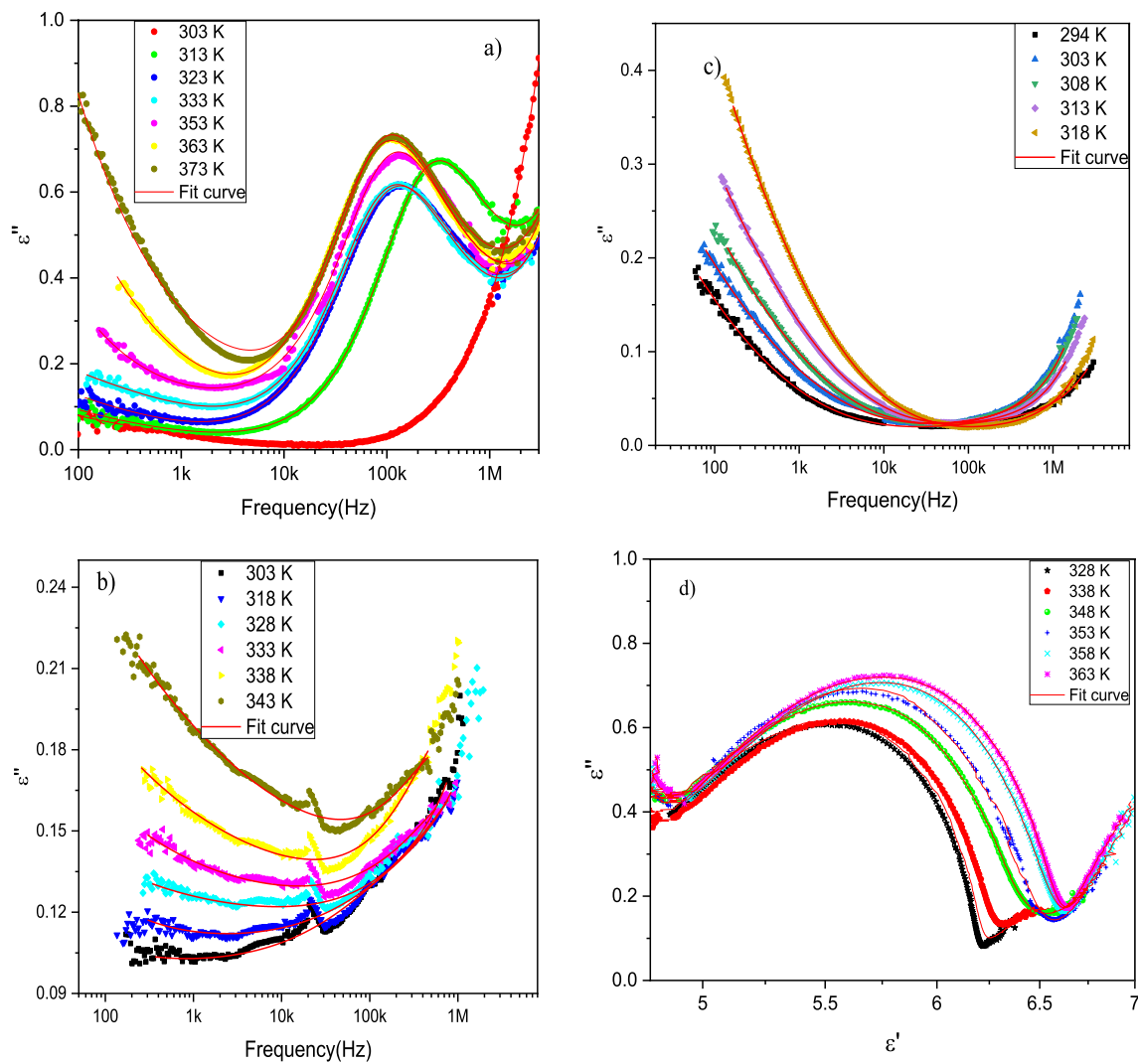
Fig. 6 Frequency dependence of the imaginary part of the dielectric permittivity, measured at different temperatures on the **a** Boc-Phe-Leu@PLLA, **b** Boc-Phe-Leu@PMMA, and **c** Boc-Phe-Leu@PCL fibers. In **d** are the corresponding Cole–Cole plots obtained at different temperatures in the case of the Boc-Phe-Leu@PLLA fibers. A clear semi-circle is visible corresponding to the relaxation process observed already in Fig. 5 and in this figure. The lines are fits to the Havriliak-Negami relaxation model as explained in the text

Maxwell–Wagner interfacial polarization [22, 23], which is associated with the existence of interfaces in the material due to the inclusion of dipeptides within the fibers, confirming their incorporation within them.

On the other hand, the real and imaginary components of the permittivity initially present a drop in the low-frequency region and then attain a slower decrease for higher frequencies. This is due to the increased difficulty of the charges to follow the applied electric field, as the frequency increases, resulting in a decrease in permittivity with increasing frequency. Additionally, a relaxation process is observed with a maximum in the imaginary component of the permittivity, which is outside of the measurement region in the three cases. However, for the Boc-Phe-Leu@ PLLA fibers, as the temperature increases, the maximum progressively moves to lower frequencies, well inside the measurement region.

For purely electronic conductivity, the electric permittivity is imaginary and given by $\varepsilon'' = \frac{\sigma_{DC}}{\varepsilon_0 \omega}$ [22], where ε_0 is the vacuum dielectric permittivity, ω is the angular frequency and σ_{DC} is the DC conductivity. For ionic charge carriers, which cause electrode or Maxwell–Wagner-polarization effects, this equation can be generalized, so that the electric conductivity contribution can be described by the equation $\varepsilon'' = \frac{\sigma_{DC}}{\varepsilon_0 \omega^s}$, where s is an exponent and $s \leq 1$ [22]. Since the conductivity

term gives high values of the imaginary component of the permittivity for low frequencies (as $\omega \to 0$), then the initial decrease of ε'', with increasing frequency is due to the electric conductivity contribution to the permittivity.

The observed relaxations are broad, indicating a distribution of relaxation times and the presence of correlated dipole behavior. Thus, to fit the electrical permittivity curves, the Havriliak–Negami (HN) model function [22–25], with one relaxation time plus a conductivity term was considered:

$$\varepsilon(\omega) = \varepsilon_\infty + \frac{\Delta\varepsilon}{\left[1 + (i\omega\tau)^\beta\right]^\gamma} + i\frac{\sigma_{DC}}{\varepsilon_0\omega^s} \tag{2}$$

where $\Delta\varepsilon$ is the intensity of the relaxation, ε_∞ is the high-frequency dielectric constant, ω is the angular frequency, τ is the relaxation time, and β and γ are coefficients of the HN function, with the constraints $0 < \beta \leq 1$ and $0 < \beta\gamma \leq 1$. For $\beta = \gamma = 1$ the HN model reduces to the Debye function, with only one relaxation time. The imaginary part of the permittivity was fitted with Eq. (2) as shown in Fig. 6, to determine the function parameters. Figure 6d, in particular, shows the Cole–Cole plot for the Boc-Phe-Leu@PLLA fibers, where clear semi-circles are visible, which are well described by the model of Eq. 1.

The σ_{DC} behavior as a function of temperature, determined from the fits to the electric permittivity, shows characteristic Arrhenius-like processes, with activation energy ($E_{a\sigma}$), given by the equation [26]:

$$\sigma \cdot T = \sigma_0 e^{-E_a/k_B T} \tag{3}$$

where T is the temperature, k_B is the Boltzmann constant and σ_0 is a constant. The activation energy can be determined from the slopes of the fittings to the curves of $\ln(\sigma T)$ as a function of the inverse of T, for the different temperature regions, as shown in Fig. 7a. Two temperature regions with different conductivity behavior are seen in the fits of Fig. 7a for Boc-Phe-Leu@PLLA and the corresponding activation energy values are shown in Table 1. For Boc-Phe-Leu@PCL and Boc-Phe-Leu@PMMA fibers only one activation energy was observed in the measured temperature region.

In the Boc-Phe-Leu@PLLA sample, an electronic contribution to DC conduction was observed, with an activation energy of $E_a = 1.12$ eV for the high-temperature region (above 323 K) and $E_a = 0.32$ eV for the low-temperature region (below 318 K). This indicates ionic conduction mediated by hydrogen ion diffusion along the molecule at high temperatures, while at low temperatures the conduction is mainly electronic, mediated through free or bound polarons [27]. The activation energies for the PCL and PMMA based nanofibers indicate polaron conduction as the main conduction mechanism in the whole temperature region.

The dielectric behavior in the frequency domain is related to that in the time domain by a Fourier transformation. For independent dipoles, with relaxation time τ_D, an exponential decay of the dipole correlation function $\phi(t) = \phi(0)e^{-t/\tau_D}$ is obtained, giving the Debye behavior $\varepsilon(\omega) = \Delta\varepsilon/(1 + i\omega\tau_D)$ in the frequency domain [22]. For a non-Debye relaxation, dipole correlations develop giving a stretched exponential behavior in the time domain described by the Kohlrausch–Williams–Watts (KWW) function:

$$\phi(t) = \phi(0)\exp\left(-\left(\frac{t}{\tau_{KWW}}\right)^{\beta_{KWW}}\right) \tag{4}$$
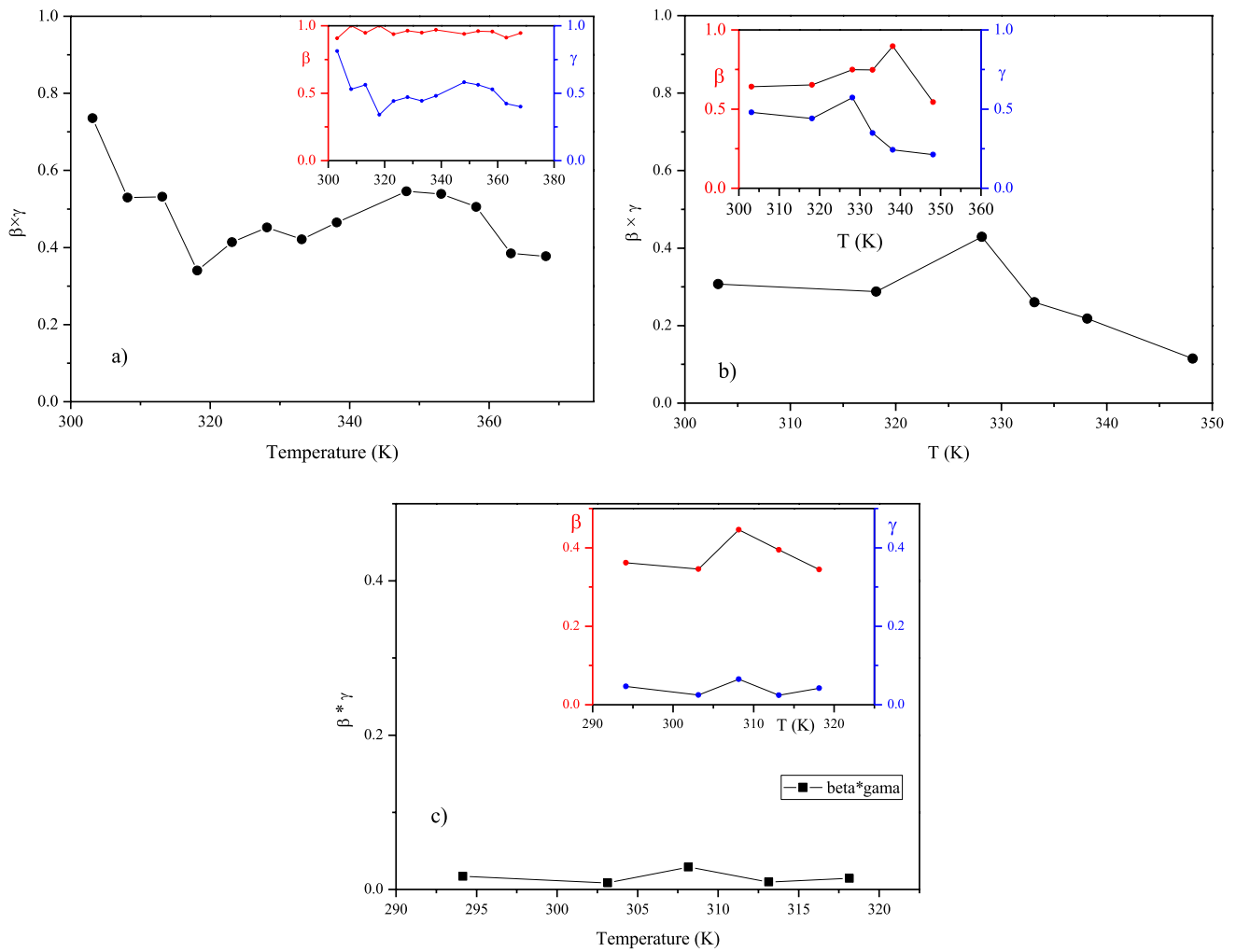
where β_{KWW} is the stretched exponential parameter and τ_{KWW} the corresponding relaxation time. β_{KWW} can be connected to the parameters β and γ of the HN function by the relation $\beta_{KWW} = \beta \times \gamma$ [28, 29]. Figure 8 shows the temperature dependence of the stretched exponential parameter, β_{KWW}, and of the β and γ Havriliak–Negami parameters. At low temperature, β_{KWW} is more Debye like, although with values well below 1 ($\beta_{KWW} \sim 0.75$). As the temperature increases, β_{KWW} slightly decreases in the three cases. The variation is mainly due to the asymmetric broadening parameter γ as shown in the insets of Fig. 8, since γ it is lower and more temperature dependent than the β parameter.

**Table 1** Activation energies (Ea) are determined from the fittings of the electric conductivity of Fig. 7

Sample	$E_{a\sigma1}$ (eV)	$E_{a\sigma2}$ (eV)
Boc-Phe-Leu@PLLA	0.32	1.12
Boc-Phe-Leu@PMMA	0.56	–
Boc-Phe-Leu@PCL	0.32	–

Fig. 7 Activation energies for the electrical conduction obtained from the fits to the imaginary component of the electrical permittivity using Eq. 1, measured at different temperatures on the a) Boc-Phe-Leu@PLLA, b) Boc-Phe-Leu@PCL and c) Boc-Phe-Leu@PMMA fibers
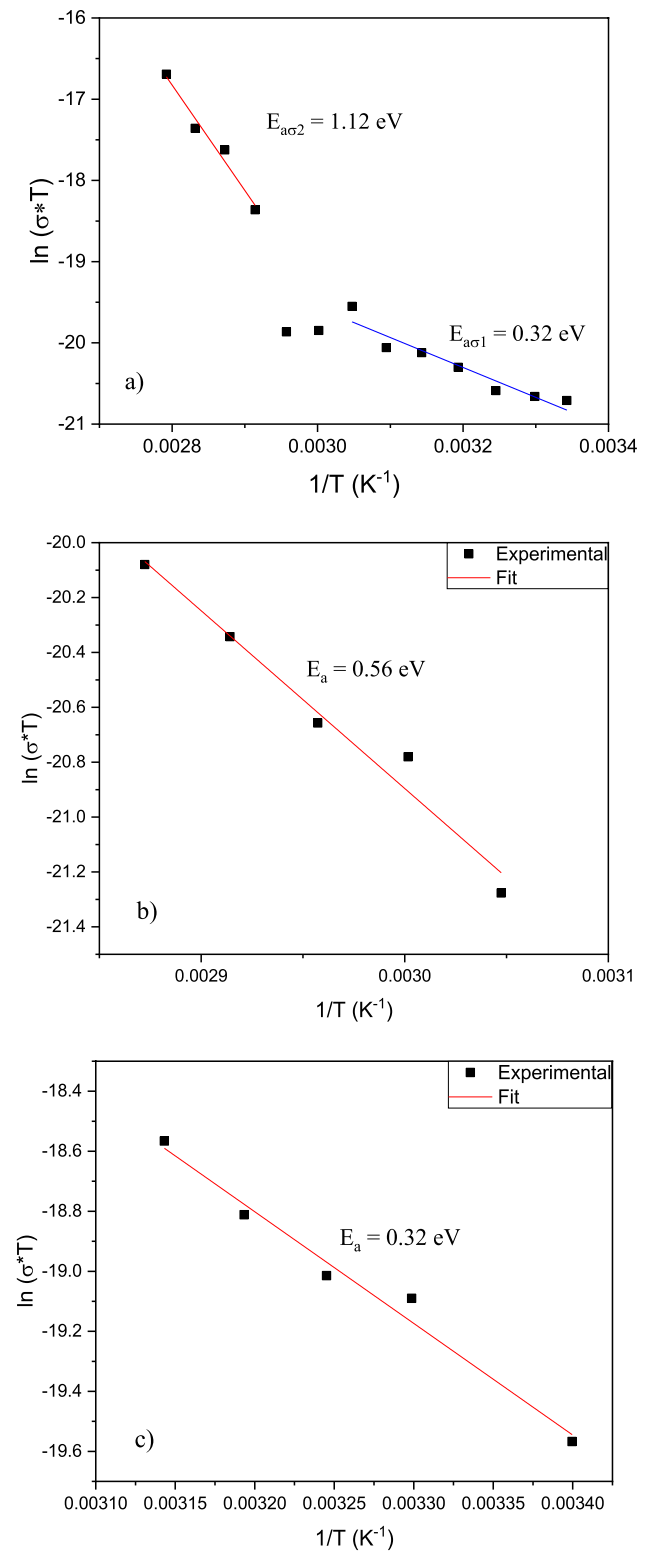
Fig. 8 Temperature dependence of the stretched exponential parameter, β_{KWW} on the **a** Boc-Phe-Leu@PLLA, **b** Boc-Phe-Leu@PCL and **c** Boc-Phe-Leu@PMMA fibers. The inset shows the individual Havriliak-Negami parameters β and γ variation with temperature
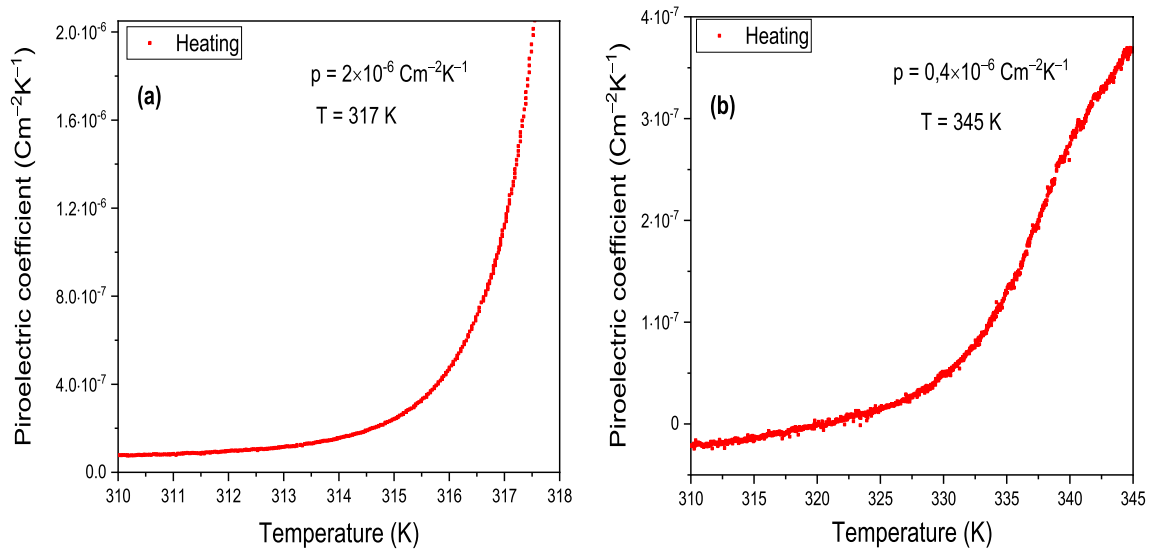
Fig. 9 Temperature dependence of the pyroelectric coefficient of the **a** Boc-Phe-Leu@PCL, **b** Boc-Phe-Leu@PMMA fibers

Table 2 Pyroelectric coefficient of several organic and semi-organic materials

Sample	p Cm^{-2}K^{-1}	T K	Refs.
Boc-Phe-Leu@PMMA (fiber mat)	0.4×10^{-6}	317	This work
Boc-Phe-Leu@PCL (fiber mat)	2×10^{-6}	345	This work
Diphenylalanine (microtubes)	2×10^{-6}	~300	[30]
Cyclo(L-Trp-L-Trp)@PLLA (fiber mat)	36×10^{-6}	315	[4]
Cyclo(L-Trp-L-Trp)@PCL (fiber mat)	35×10^{-6}	323	[4]
[a]DabcoHReO$_4$@PVA (fiber mat)	8.5×10^{-6}	300	[14]
[b]TGS (Single crystal)	35×10^{-6}	322	[31]

[a]1,4-diazabicyclo [2.2.2]-octane perrhenate at poly (vinyl alcohol)

[b]Triglycine sulphate

3.4 Pyroelectric properties

Figure 9a, presents the values of the pyroelectric coefficient as a function of temperature, for Boc-Phe-Leu@PCL nanofibers. From the graph, it can be inferred that the pyroelectric coefficient exhibits a constant behavior until approximately 313 K, beyond which it starts to increase rapidly, reaching the maximum value at 317 K. The pyroelectric coefficient is a value of 2×10^{-6} Cm^{-2} K^{-1} at the temperature of 317 K. On the other hand, for Boc-Phe-Leu@PMMA nanofibers the pyroelectric coefficient obtained is 0.4×10^{-6} Cm^{-2} K^{-1} at temperature of 345 K, as shown in Fig. 9b, being an order of magnitude lower than that obtained when the dipeptide is incorporated into PCL.

We may therefore conclude that the incorporation of the dipeptide in a PCL polymer matrix favored the manifestation of its polar proprieties.

Recently, we have reported the pyroelectric coefficient of Cyclo (L-Trp-L-Trp)@PLLA and Cyclo (L-Trp-L-Trp)@PCL nanofibers [4], whose values are, respectively, 36×10^{-6} Cm^{-2}K^{-1} at 315 K and 35×10^{-6} Cm^{-2}K^{-1} at 323 K, which is an order of magnitude higher than that reported in this work for Boc-Phe-Leu@PCL. Significantly, a study reported a pyroelectric coefficient of approximately 2×10^{-6} Cm^{-2}K^{-1} for a diphenylalanine microtubes [30] that is the same reported in this work for Boc-Phe-Leu@PCL. Table 2 presents a summary of the above-mentioned pyroelectric coefficients. The results demonstrate the potential of these nanofibers to utilize thermal energy effectively at room temperature, positioning them as promising candidates for a variety of energy conversion applications.

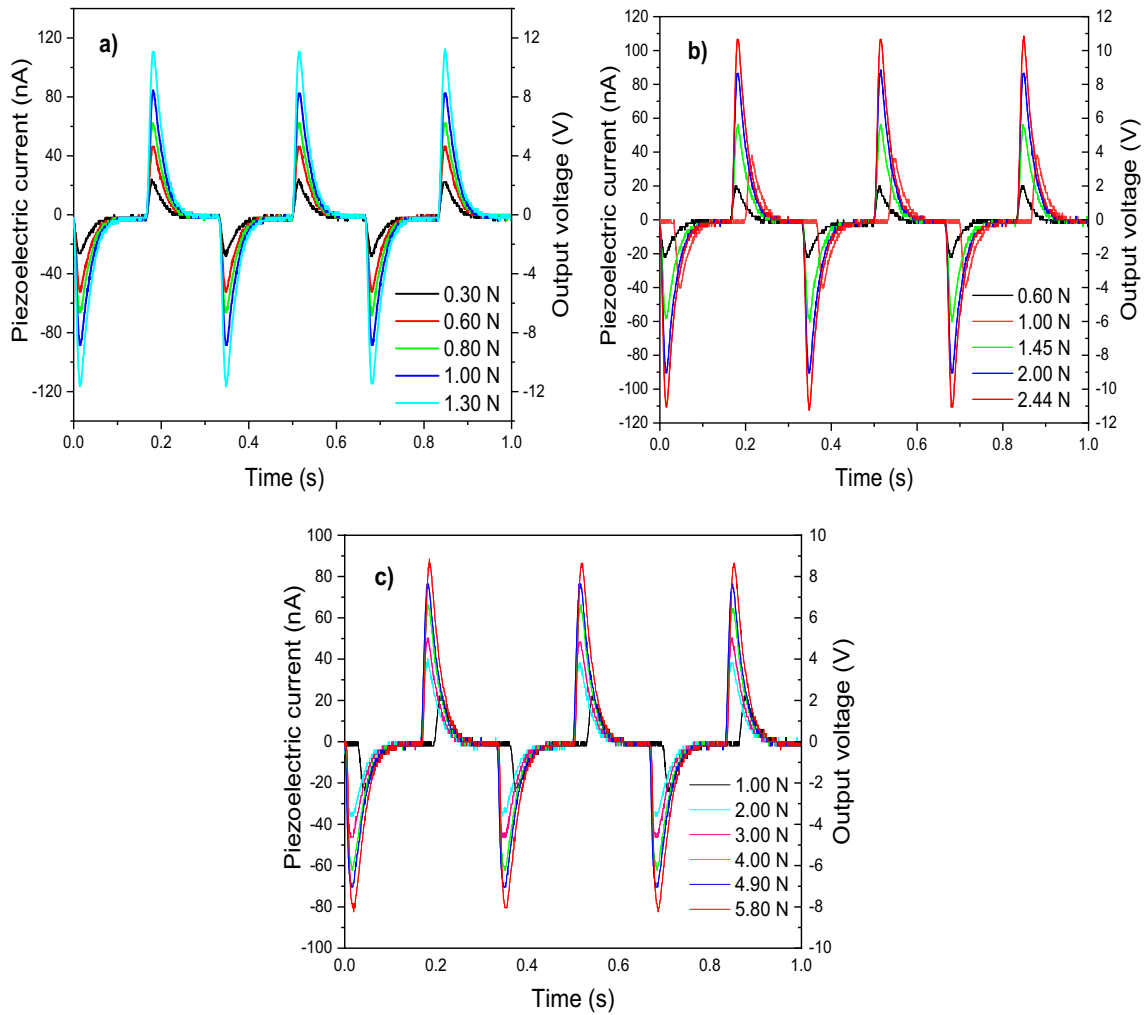## 3.5 Piezoelectric properties

Figure 10 represents the piezoelectric current and the output voltage as a function of time for the Boc-Phe-Leu@PLLA, Boc-Phe-Leu@PMMA and Boc-Phe-Leu@PCL samples. It can be observed that an increase in the applied force results in a proportional increase in both current and output voltage. The intensity of the output signal for each applied force does not show significant deviations, remaining constant over time.

A linear fit was performed to confirm the relationship between the current and the applied force, as shown in Fig. 11. The linear fits show a positive and linear trend, reinforcing the direct relationship between applied force and piezoelectric current. This confirms that an increase in force results in a proportional increase in piezoelectric current. The inset in Fig. 11 shows the schematic circuit used to measure the maximum output current.

The effective piezoelectric coefficient of the Boc-Phe-Leu@PLLA nanofibers was determined for each applied force, resulting in an average value of 85 pCN^{-1}. For Boc-Phe-Leu@PMMA, the average measured effective piezoelectric coefficient was 45 pCN^{-1}, while for Boc-Phe-Leu@PCL it was 15 pCN^{-1}.

For the Boc-Phe-Leu@PMMA and Boc-Phe-Leu@PCL samples, it is important to emphasize that it is the dipeptide molecule Boc-Phe-Leu that contributes to the generation of piezoelectric current and output voltage. The PMMA and PCL polymers themselves do not possess intrinsic piezoelectric properties.

Fig. 10 Piezoelectric current and output voltage as a function of time for the nanofibers **a** Boc-Phe-Leu@PLLA, **b** Boc-Phe-Leu@PMMA and **c** Boc-Phe-Leu@PCL fibers

Fig. 11 Piezoelectric current as a function of the applied force and its linear fit for. Boc-Phe-Leu@PLLA, Boc-Phe-Leu@PMMA and Boc-Phe-Leu@PCL fibers. The inset shows the schematic circuit used to measure the maximum output current
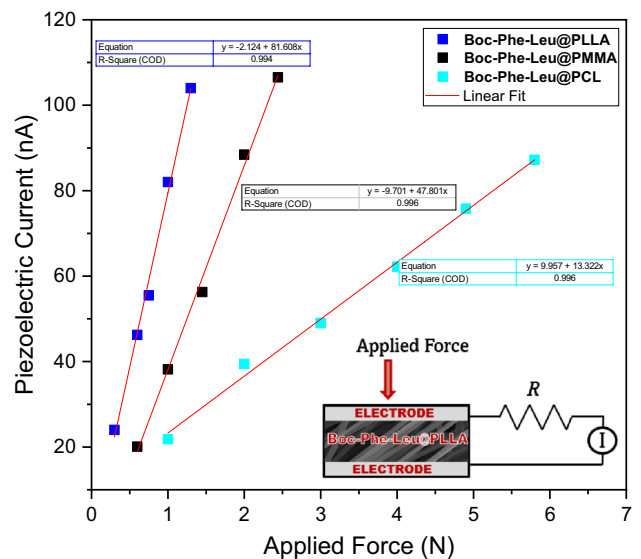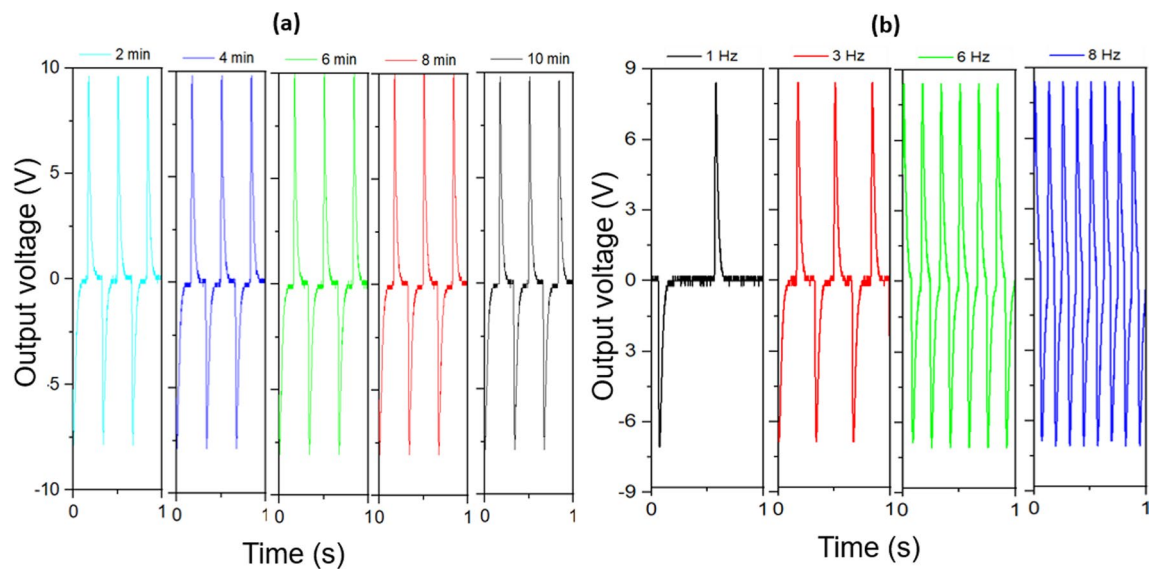
Fig. 12 Variation of the output voltage for Boc-Phe-Leu@PLLA nanofibers **a** over a 10-min time interval and **b** for different frequencies

Table 3 Parameters of the piezoelectric nanogenerator for several nanofiber mats

Nanogenerator	d_{eff} pCN^{-1}	Force/Area (Nm^{-2})	g_{eff} (VmN^{-1})	Power Density (μWcm^{-2})	Refs.
Boc-Phe-Leu@PLLA (fiber mat)	85	1×10^3	1.5	0.10	This work
Boc-Phe-Leu@PMMA (fiber mat)	45	1.5×10^3	1.1	0.10	This work
Boc-Phe-Leu@PCL (fiber mat)	15	3×10^3	0.4	0.07	This work
Boc-PhePhe@PLLA (fiber mat)	8.4	4×10^3	0.3	2.3	[11]
Boc-PheTyr@PLLA (fiber mat)	7	4×10^3	0.3	1.0	[11]
Boc-pNPhe$p$NPhe@PLLA (fiber mat)	16	4×10^3	0.6	9.0	[11]

Fig. 13 Assembly scheme of the piezoelectric nanogenerator, using the Boc-Phe-Leu@PLLA nanofiber mat as active material
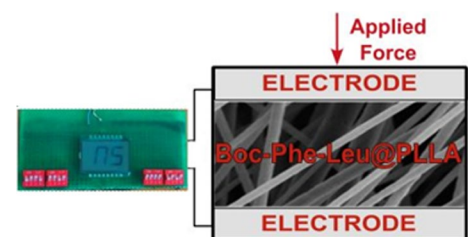
The effective coefficient is higher in Boc-Phe-Leu@PLLA, since the polymer PLLA is piezoelectric, with an effective coefficient of ~ 10 pCN^{-1} [32]. So, the incorporation of the dipeptide clearly enhances the piezoelectric response of the fibers with the PLLA polymer.

We further studied the variation of the piezoelectric signal with frequency and time in order to access the stability of the piezoelectric response. For this, the Boc-Phe-Leu@PLLA sample was chosen in light of its application in a piezoelectric energy harvesting device, as it had the highest piezoelectric coefficient. Figure 12a shows the output piezoelectric voltage for different time intervals. It can be observed that over a 10-min time interval, the intensity of the output voltage exhibits insignificant variation. This indicates high stability of the fibers over time, as the output voltage response remains nearly constant. This observation suggests that the fibers have the ability to maintain a consistent and predictable response, even when subjected to constant forces and the same frequency over time.

For the same sample, Boc-Phe-Leu@PLLA, the behavior of the output voltage was evaluated for different frequencies, of 1, 3, 6, and 8 Hz, while keeping the force constant within the same time interval, as shown in Fig. 12b. The output voltage remained constant at all applied frequencies for the fibers.

A very importantly parameter for application of the nanofiber mats as energy harvesters, is the piezoelectric voltage coefficient $g_{eff} = d_{eff}/(\varepsilon'\varepsilon_0)$ VmN^{-1}, a figure of merit that quantifies the materials adequacy as a piezoelectric sensor. Another important quantity to highlight is the power density released by the nanofiber mat, given by $W = RI^2/A$ (μWcm^{-2}), where R = 100 MΩ is the resistance and A is the electrode area. The calculated values are listed in Table 3.

To test the piezoelectric energy harvesting response of the produced nanofibers, a circuit was assembled using a liquid crystal display (LCD). In this circuit, the fibers were connected to the LCD to demonstrate the functioning of a piezoelectric nanogenerator. The assembly diagram is shown in Fig. 13.

In the experimental assembly, the nanofibers are connected as a parallel plate capacitor. In the circuit, the conductors of the LCD screen were connected to the fiber mat. By exerting a mechanical force on the fibers, an output voltage is generated due to the piezoelectric effect. The resulting electric current from the output voltage was responsible for supplying the necessary energy for the operation of the LCD screen, as shown in Fig. 13. For comparison, a similar assembly was performed using PLLA nanofibers, without the inclusion of the dipeptide, which lead to a much worse energy harvesting performance. The obtained results revealed a significant improvement in the LCD screen signal when the nanofibers with the incorporated dipeptide were used, indicating that the presence of the dipeptide inside the polymer matrix resulted in higher efficiency in generating the piezoelectric response.

We may conclude that linear Boc-Phe-Leu dipeptide nanocrystals embedded into biopolymers, in particular PCL, and fabricated by the electrospinning technique, form easily handled nanomaterials systems capable of performing as piezoelectric energy nanogenerators with significant piezoelectric voltage coefficients.

4 Conclusions

Composite micro/nanofibers were produced by electrospinning, incorporating the linear chiral dipeptide Boc-Phe-Leu inside a polymeric matrix, with different base polymers (PLLA, PMMA and PCL). The scanning electron microscopy studies showed that the micro/nanofibers were uniform, aligned and well-oriented, with diameters ranging from 0.56 to 1.68 µm. The bandgap energies of Boc-Phe-Leu and of the composite fibres were determined and ranged between 4 and 5 eV, indicating that the materials behave as (bio)organic semiconducting dielectrics. The dielectric properties of the samples were studied in relation to temperature and frequency. An increase in the dielectric constant with increasing temperature was observed, due to the greater availability of energy to move charges in the direction of the applied alternating electric field. The presence of Maxwell–Wagner interfacial polarization indicated the incorporation of the peptide in the fibres. The Havriliak–Negami model was applied to fit the imaginary component of the electric permittivity as a function of frequency, obtaining parameters related to the contribution of DC conduction. The role of polaron and ionic conduction, depending on the polymeric matrix of the fibers was identified. Their pyroelectric and piezoelectric responses were also evaluated. Throughout the study, it was possible to confirm that polymeric micro/nanofibers have the ability to act as piezoelectric energy generators, converting mechanical energy from a periodically applied mechanical force. In this respect, Boc-Phe-Leu@PLLA nanofibers exhibited the highest values of the effective piezoelectric coefficient, reaching 85 pC/N when compared with other Boc protected linear dipeptides. As such, these combined results confirm the ability of polymeric micro/nanofibers to function as nanogenerators of piezoelectric energy, enabling their application in portable and wearable devices, such as smartwatches, motion sensors, health monitoring systems, among others.

Author contributions Conceptualization, AH, RMFB and EdMG; investigation, AH, RMFB, DS, BS, BA, JO; writing-original draft preparation, AH, RMFB and BA; writing-review and editing, RMFB, EdMG, BA and MB; supervision, RMFB, EdMG and BA; project administration, RMFB and BA; funding acquisition, RMFB and BA All authors have read and agreed to the published version of the manuscript.

Declarations

competing interests The authors declare no conflict of interest.

References

1. Wang ZL. Triboelectric nanogenerators as new energy technology for self-powered systems and as active mechanical and chemical sensors. ACS Nano. 2013;7:9533–57. https://doi.org/10.1021/nn404614z.
2. Askari H, Xu N, Groenner Barbosa BH, Huang Y, Chen L, Khajepour A, Chen H, Wang ZL. Intelligent systems using triboelectric, piezoelectric, and pyroelectric nanogenerators. Mater Today. 2022;52:188–206. https://doi.org/10.1016/j.mattod.2021.11.027.
3. Li T, Lu XM, Zhang MR, Hu K, Li Z. Peptide-based nanomaterials: self-assembly, properties and applications. Bioact Mater. 2022;11:268–82. https://doi.org/10.1016/J.BIOACTMAT.2021.09.029.
4. Santos D, Baptista RMF, Handa A, Almeida B, Rodrigues PV, Torres AR, Machado A, Belsley M, de Matos GE. Bioinspired cyclic dipeptide functionalized nanofibers for thermal sensing and energy harvesting. Materials. 2023;16:2477. https://doi.org/10.3390/ma16062477.
5. Vasilev S, Zelenovskiy P, Vasileva D, Nuraeva A, Shur VY, Kholkin AL. Piezoelectric properties of diphenylalanine microtubes prepared from the solution. J Phys Chem Solids. 2016;93:68–72. https://doi.org/10.1016/j.jpcs.2016.02.002.
6. Baptista RMF, De Matos GE, Raposo MMM, Costa SPG, Lopes PE, Almeida B, Belsley MS. Self-assembly of dipeptide Boc-diphenylalanine nanotubes inside electrospun polymeric fibers with strong piezoelectric response. Nanoscale Adv. 2019;1:4339–46. https://doi.org/10.1039/c9na00464e.
7. Gazit E. Self-assembled peptide nanostructures: the design of molecular building blocks and their technological utilization. Chem Soc Rev. 2007;36:1263–9. https://doi.org/10.1039/B605536M.
8. Doria G, Conde J, Veigas B, Giestas L, Almeida C, Assunção M, Rosa J, Baptista PV. Noble metal nanoparticles for biosensing applications. Sensors. 2012;12:1657–87. https://doi.org/10.3390/s120201657.
9. Subbalakshmi C, Basak P, Nagaraj R. Self-assembly of t-butyloxycarbonyl protected dipeptide methyl esters composed of leucine, isoleucine, and valine into highly organized structures from alcohol and aqueous alcohol mixtures. Biopolymers. 2017;108: e23033. https://doi.org/10.1002/bip.23033.
10. Zhao L, Yan X. Supramolecular self-assembly: a facile way to fabricate protein and peptide nanomaterials. In: Em: artificial protein and peptides nanofibers: design, fabrication, characterization and applications. Woodhead Publishing; 2020. p. 3–21.
11. Baptista RMF, Lopes PE, Rodrigues ARO, Cerca N, Belsley MS, de Matos GE. Self-assembly of Boc-p-nitro-l-phenylalanyl-p-nitro-l-phenylalanine and Boc-l-phenylalanyl-l-tyrosine in solution and into piezoelectric electrospun fibers. Mater Adv. 2022;3:2934–44. https://doi.org/10.1039/d1ma01022k.
12. Tulip PR, Clark SJ. Dielectric and vibrational properties of amino acids. J Chem Phys. 2004;121:5201–10. https://doi.org/10.1063/1.1781615.
13. Tulip PR, Clark SJ. Lattice dynamical and dielectric properties of L-amino acids. Phys Rev B. 2006;74:064301. https://doi.org/10.1103/PhysRevB.74.064301.
14. Isakov D, de Matos GE, Almeida B, Kholkin AL, Zelenovskiy P, Neradovskiy M, Shur VY. Energy harvesting from nanofibers of hybrid organic ferroelectric dabcoHReO4. Appl Phys Lett. 2014. https://doi.org/10.1063/1.4862437.
15. Jenkins K, Kelly S, Nguyen V, Wu Y, Yang R. Piezoelectric diphenylalanine peptide for greatly improved flexible nanogenerators. Nano Energy. 2018;51:317–23. https://doi.org/10.1016/j.nanoen.2018.06.061.
16. Guerin S, Stapleton A, Chovan D, Mouras R, Gleeson M, McKeown C, Noor MR, Silien C, Rhen FMF, Kholkin AL, Liu N, Soulimane T, Tofail SAM, Thompson D. Control of piezoelectricity in amino acids by supramolecular packing. Nat Mater. 2018;17:180–6. https://doi.org/10.1038/nmat5045.
17. Kholkin A, Amdursky N, Bdikin I, Gazit E, Rosenman G. Strong piezoelectricity in bioinspired peptide nanotubes. ACS Nano. 2010;4:610–4. https://doi.org/10.1021/nn901327v.
18. Bystrov VS, Bdikin IK, Singh B. Piezoelectric and ferroelectric properties of various amino acids and tubular dipeptide nanostructures: Molecular modelling. Nanomater Sci Eng. 2020;2:11–24. https://doi.org/10.34624/nmse.v2i1.8259.
19. O'Donnell J, Sarkar SM, Guerin S, Borda GG, Silien C, Soulimane T, Thompson D, O'Reilly E, Tofail SAM. Piezoelectricity in the proteinogenic amino acid L-leucine: a novel piezoactive bioelectret. IEEE Trans Dielectr Electr Insul. 2020;27:1465–8. https://doi.org/10.1109/TDEI.2020.008908.
20. Jana P, Maity S, Maity SK, Ghorai PK, Haldar D. Photo-induced charge-transfer complex formation and organogelation by a tripeptide. Soft Matter. 2012;8:5621. https://doi.org/10.1039/c2sm25062d.
21. Schneider CA, Rasband WS, Eliceiri KW. NIH Image to ImageJ: 25 years of image analysis. Nat Methods. 2012;9:671–5. https://doi.org/10.1038/nmeth.2089.
22. Kremer F, Schönhals A. Broadband dielectric spectroscopy. Springer; 2003.
23. Silva BM, Oliveira J, Rebelo T, Isfahani VB, Rocha-Rodrigues P, Lekshmi N, Belo JH, Deepak FL, Lopes AML, Araújo JP, Almeida BG. Synthesis, structural and dielectric properties of Ca3Mn2O7 thin films prepared by pulsed laser deposition. Mater Res Bull. 2023;158:112066. https://doi.org/10.1016/j.materresbull.2022.112066.

24. Havriliak S, Negami S. A complex plane representation of dielectric and mechanical relaxation processes in some polymers. Polymer (Guildf). 1967;8:161–210. https://doi.org/10.1016/0032-3861(67)90021-3.

25. Poplavko Y. Broadband dielectric spectroscopy. Woodhead Publishing; 2021. https://doi.org/10.1016/b978-0-12-823518-8.00001-3.

26. Nuernberg RB. Numerical comparison of usual Arrhenius-type equations for modeling ionic transport in solids. Ionics (Kiel). 2020;26:2405–12. https://doi.org/10.1007/s11581-019-03243-7.

27. Franchini C, Reticcioli M, Setvin M, Diebold U. Polarons in materials. Nat Rev Mater. 2021;6:560–86. https://doi.org/10.1038/s41578-021-00289-w.

28. Alvarez F, Alegra A, Colmenero J. Relationship between the time-domain Kohlrausch-Williams-Watts and frequency-domain Havriliak-Negami relaxation functions. Phys Rev B. 1991;44:7306–12. https://doi.org/10.1103/PhysRevB.44.7306.

29. Górska K, Horzela A, Bratek Ł, Dattoli G, Penson KA. The Havriliak-Negami relaxation and its relatives: the response, relaxation and probability density functions. J Phys A Math Theor. 2018;51:135202. https://doi.org/10.1088/1751-8121/aaafc0.

30. Esin A, Baturin I, Nikitin T, Vasilev S, Salehli F, Shur VY, Kholkin AL. Pyroelectric effect and polarization instability in self-assembled diphenylalanine microtubes. Appl Phys Lett. 2016. https://doi.org/10.1063/1.4962652.

31. Ghane-Motlagh R, Kroener M, Goldschmidtboeing F, Danilewsky AN, Woias P. A dynamic method for the measurement of pyroelectric properties of materials. Smart Mater Struct. 2018;27:084004. https://doi.org/10.1088/1361-665X/aac0b3.

32. Udovč L, Spreitzer M, Vukomanović M. Towards hydrophilic piezoelectric poly-L-lactide films: optimal processing, post-heat treatment and alkaline etching. Polym J. 2020;52:299–311. https://doi.org/10.1038/s41428-019-0281-5.

Publisher's Note Springer Nature remains neutral with regard to jurisdictional claims in published maps and institutional affiliations.